JOURNAL OF AIRCRAFT
Vol. 44, No. 6, November–December 2007

Lateral Response of Nose-Wheel Landing Gear System to Ground-Induced Excitation

Niranjan K. Sura*
Aeronautical Development Agency, Bangalore 560 017, India
and
S. Suryanarayan†
Indian Institute of Technology, Bombay, Mumbai 400 076, India

DOI: 10.2514/1.28854

Nose-wheel landing gears can become laterally unstable during takeoff, taxiing, and landing, exhibiting divergent coupled lateral flexural and torsional oscillations called shimmy. The system stability is governed by the gear and tire dynamic characteristics, system nonlinearities, and vibratory modes of the vehicle, as well as by the degree of coupling that exists between these modes. Ground unevenness can produce significant lateral excitation on the landing gear and results in adversely impacting its lateral stability. To evaluate a nose-wheel landing gear system for its stability and response, it is necessary to model system components to capture the contributions of the landing gear structure, the tire, wheel configuration, system nonlinearities, and its interaction with the runway. This paper examines the lateral response of linear and nonlinear simplified nose-wheel landing gear models to ground-induced lateral excitation. Considering torsional free play as the source of nonlinearity and external excitation due to runway roughness, modeling and analysis of nose-wheel landing gear shimmy is presented. The spatial variation of the runway surface is modeled as a continuous profile, obtained as a combination of sinusoids to represent a randomlike ground-induced excitation with the specified power spectral density. Time-domain simulation studies on the linear landing gear system show that unacceptable levels of lateral accelerations may be caused even at subcritical velocities. Studies on nonlinear nose-wheel landing gear systems bring out the fact that the free play can result in a significant reduction of the critical shimmy velocity and the need for such simulations in the subcritical ranges of velocities.

Nomenclature

C	=	coefficient of tire yaw
C_S	=	structural lateral damping coefficient
C_{Sh}	=	equivalent viscous damping coefficient in torsion
C_α	=	rotational damping coefficient in the direction of α
C_Δ	=	tire lateral damping coefficient
C_θ	=	equivalent structural damping coefficient in torsion
C_ψ	=	torsional tire damping coefficient
C_1	=	tire time constant
F_N	=	side force due to lateral flexibility of the tire
$F_{z\mathrm{ex}}$	=	vertical excitation at the wheel contact point due to runway roughness
I	=	moment of inertia of the wheel-strut assembly about the gear vertical axis
I_P	=	polar moment of inertia of the wheel assembly
I_α	=	moment of inertia of the wheel assembly about the fore and aft axis (roll axis) at the wheel hub
K_S	=	lateral stiffness of the landing gear
K_{Zt}	=	vertical stiffness of the tire
K_α	=	roll stiffness coefficient (in the direction of α)
K_Δ	=	lateral stiffness of the tire
K_θ	=	torsional stiffness of the landing gear
K_ψ	=	tire torsional stiffness
L	=	distance of axis of wheel rotation from the gear vertical axis
L_{aw}	=	distance of the wheel plane of rotation from the gear vertical axis
L_{cg}	=	distance of the center of gravity of the wheel-strut assembly from the gear vertical axis
L_G	=	geometric trail length
M_{dw}	=	roll moment due to dual-wheel configuration
M_{sw}	=	roll moment due to single-wheel configuration
M_α	=	moment in the wheel-roll direction
$M_{\alpha\mathrm{ex}}$	=	tire yawing (cornering) moment due to tire twist
M_θ	=	torsional moment about the strut axis
m	=	mass of the wheel-strut assembly
N	=	landing gear vertical reaction
P	=	ground-profile power spectral density function
R	=	rolling radius of the wheel tire
t	=	dimensional time
V	=	aircraft forward-taxi velocity
V_{Cr}	=	critical shimmy velocity
V_{ts}	=	tire contact point velocity (velocity of tire slip)
y	=	strut lateral deflection
Z	=	random ground profile expressed in time/spatial domain in the vertical direction
α	=	wheel-roll degree of freedom about the fore–aft axis through the trail arm
α_{ex}	=	roll excitation due to runway roughness
γ	=	attitude angle of the gear, positive wheel forward
Δ	=	tire-contact-patch centerline lateral deflection with respect to the wheel center plane
Δ_{Zt}	=	vertical tire deflection
η_{rc}	=	ground roughness constant
θ	=	torsional rotation about the strut vertical centerline
θ_{fp}	=	free play in the rotation of the wheel
μ_r	=	rolling friction coefficient
ν	=	ground correlation constant
ψ	=	tire torsional deformation about the vertical axis
Ω	=	ratio of landing gear torsional frequency to structural frequency, ω_θ/ω_S

Received 14 November 2006; revision received 6 February 2007; accepted for publication 5 June 2007.

*Scientist, National Control Law Team, Integrated Flight Control Systems Directorate.

†Professor (Retired), Aerospace Engineering Department.

ω = spatial frequency
ω_{Cr} = critical shimmy frequency
ω_o = spatial cutoff frequency
ω_S = uncoupled landing gear lateral frequency, $\sqrt{(K_S/m)}$
ω_θ = uncoupled landing gear torsional frequency, $\sqrt{(K_\theta/I)}$

I. Introduction

AIRCRAFT dynamics during taxiing, takeoff, and landing involve participation of the landing gear, which plays a crucial role in ensuring safety and comfort. Hence, the study of the dynamics of the aircraft nose-wheel landing gear (NLG) for stability and response is an important component of the design and certification process of aircraft. NLG vibrations include brake-induced vibrations and self-induced lateral oscillations referred to as shimmy. Shimmy is a self-excited instability that may occur during takeoff, taxiing, and landing, involving mainly three vibratory motions: lateral displacement of the strut, rotation of the wheel assembly about the vertical axis (yaw), and rotation about the fore and aft axis (roll). The basic cause of shimmy is the energy transfer from the forward motion of the aircraft to the lateral vibratory modes of the landing gear system through the contact force between the tires and the ground. The stability of the system depends on the dynamic characteristics of the gear, tires, and vibratory modes of the vehicle as a whole, as well as the degree of coupling that exists between various modes of these components. Shimmy may be caused by a number of conditions such as low torsional stiffness of the strut, free play in the gear, wheel imbalance, or worn parts. Landing gears that shimmy are unacceptable, and in fact, a severe occurrence of shimmy can damage the landing gear and its attaching structure, resulting in significant repair costs. At speeds close to critical (shimmy) velocity, small motions may become unstable and grow, and in severe cases, the pilot may not be able to take corrective action, leading to the failure of the gear. It is therefore necessary that NLG designs ensure adequate margins between the taxi speeds and the critical velocity of shimmy under all operating conditions. Unlike the NLG, because the main landing gear does not have the swivel degree of freedom and associated low torsional rigidity, it does not have shimmy instability, and its torsional response to lateral excitation is not significant enough to influence the lateral dynamics of the aircraft taxiing on ground.

To evaluate the landing gear system for its stability and response, it is necessary to develop an adequately representative model, integrating the various models of the system components, capturing the contributions of the landing gear structure, the tire, wheel configuration, steering mechanism, runway interaction, free play, friction, and other system nonlinearities. There are studies [1–4] on analytical models of the NLG system that examine the effects of NLG geometry as well as landing gear structural and tire parameters. Moreland [1] presented a description of a landing gear system having strut deflection, swivel angle, tire deflections, linkage strains, and airframe motion as degrees of freedom (DOF). His model accounts for torsional and lateral rigidities of the strut, wheel moment of inertia, weight of the strut, and tire elasticity. Walter and Howard [2] presented an analytical model to study the effect of the geometry of caster-system inertia distribution, considering a single-wheel configuration. Krabacher [3,4] presented detailed mathematical models with tire lateral deflection, tire twist, swivel angle, strut deflection, and wheel tilt as DOF, taking into account structural inertias and flexibilities.

Nonlinearities in the landing gear make the evaluation of the shimmy phenomenon more complex and its prediction more difficult. It is necessary to incorporate landing gear nonlinearities to obtain accurate estimates of the critical velocity of shimmy. Krabacher [3,4] analyzed landing gear models, accounting for torsional free play and coulomb friction. He identified critical nonlinear parameters in the models by examining the sensitivity of these parameters to numerical variation. There have also been studies on modeling [5–8] and evaluation [9–13] of nonlinear models for the analysis of nose-wheel shimmy. It has been observed that the linear NLG model has a region of stable response, with the critical value of the forward velocity as its upper boundary [9,10]. The nonlinear NLG models, on the contrary, displayed a more complex behavior with limit-cycle oscillations for some cases, over a range of velocity values [11–13]. No external excitation was considered in these studies. It would be interesting to examine whether the presence of external excitation alters the stability characteristics and boundaries of the nonlinear systems and how the limit-cycle amplitudes are affected by the external excitation. Runway-induced excitation has been an important subject of study in the dynamic response of landing gears. Runway roughness will, in general, produce longitudinal as well as lateral excitations. For linear NLG models, runway-induced excitations available as power spectral density (PSD) functions can directly be used to obtain the response spectrum. However, for nonlinear NLG systems, the response needs to be simulated in the time domain. For such studies, modeling of the ground profile is an essential requirement for simulation of system response.

In general, ground profiles are continuous and irregular. The ground unevenness can be assumed as a homogeneous process with zero mean and for which the frequency content can be represented by a PSD function [14–16]. Because ground-profile variation does show statistical regularity to an extent, it can be modeled as a stationary Gaussian process. The spatial variation of the profile can be modeled as a continuous profile, obtained as a combination of sinusoids to represent a randomlike ground-induced excitation with the specified power spectral density [15,16]. The nonhomogeneous ground profile can be expressed as the sum of a variable mean and a zero mean random unevenness, and response samples can be generated to form an ensemble and can be processed to obtain the second-order response statistics during landing and takeoff [14]. Characterization of ground unevenness and generation of random ground profiles have also been reported in the literature [14–19].

This paper examines the lateral response of linear and nonlinear NLG models to ground-induced lateral excitation. Considering torsional free play as a source of nonlinearity, modeling and analysis of shimmy is presented. For prepared surfaces, the ground roughness model described by a PSD function used in [14,15] is found suitable to adequately represent the measured profile. In the current work, the preceding model is used to generate randomlike ground profiles using an algorithm based on superposition of sinusoids with random phases [20].

II. Ground-Profile Modeling

For the simulation of the response of wheeled systems to ground excitations, the ground profile as a function of spatial coordinates along the travel path can be converted to functions of time for a given forward velocity. Let the random ground profile be expressed as $Z(x)$ in the space domain, where x is the position along the path at time t. This random profile [14,15] can be described to the second order by the correlation and is given by

$$\begin{aligned} P(\omega) &= \frac{\eta_{rc}}{\omega^2+\nu^2} \quad \omega \leq \omega_o \\ &= 0 \qquad\quad\ \omega > \omega_o \end{aligned} \tag{1}$$

where ω is the spatial frequency, ω_o is the cutoff frequency, η_{rc} is the roughness constant, and ν is the correlation constant. The PSD function given by Eq. (1) gives a simple representation of the random ground profile in which the ground roughness is measured in vertical direction. This expression can be used to generate a range of runway profiles for roughness conditions from poor to good by an appropriate choice of roughness and correlation constants. The spectrum can be considered as a combination of an infinite number of sinusoidal components of various power levels. Choosing the phase values of these sinusoids randomly and superposing these sinusoids, the ground spectrum can be converted to a spatial ground profile, as shown in Fig. 1. Choosing the random phase ϕ of the sinusoid between $-\pi$ and $+\pi$ with frequency ω chosen, the random ground profile can be expressed in the space domain [16] as

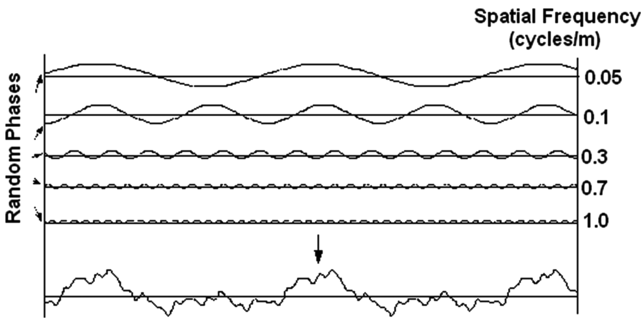

Fig. 1 Random ground profile as a superposition of sinusoids with random phases

$$Z(x) = \sum_{i=1}^{\infty}[\sqrt{P(\omega_i)\,\mathrm{d}\omega}]\cos(2\pi\omega_i x + \phi_i) \tag{2}$$

The ground profile thus generated in space is converted into a function of time using the forward velocity V of the vehicle, which is given by

$$Z(t) = \sum_{i=1}^{\infty}[\sqrt{P(\omega_i)\,\mathrm{d}\omega}]\cos(2\pi V\omega_i t + \phi_i) \tag{3}$$

Figure 2 shows typical ground-profile PSD for a rough-correlated ground ($\eta_{\mathrm{rc}} = 0.5 \times 10^{-4}$ and $\nu = 0.5$). Runway profiles are generated for different values of roughness and correlation constants for a period of 15 s for the taxi run velocity, up to 80 m/s at an interval for 1 m/s. The nature of profiles generated ranges from smooth-correlated to rough-uncorrelated by choosing different combinations of roughness and correlation constants. For typical combinations of roughness and correlation constants, Figs. 3–6 show smooth-correlated, smooth-uncorrelated, rough-correlated, and rough-uncorrelated profiles, respectively, as functions of runway length and as a function of time ($V = 10$ m/s). For the preceding roughness and correlation constant combinations, Fig. 7 shows runway excitation amplitudes as a function of time at $V = 10$ m/s to the same scale. Here, 10 m/s represents a low-speed taxi run and the value is chosen to demonstrate the profiles in time domain. For the class of aircraft considered, the takeoff and landing velocities are about 80 and 50 m/s, respectively.

III. Ground Excitation Modeling

After the generation of track/ground profile as a function of time, the vertical excitation $F_{z\mathrm{ex}}$ at the wheel contact point at time t can be computed as

$$F_{z\mathrm{ex}} = \frac{N_{\mathrm{ng}}}{g}\ddot{Z}(t) \tag{4}$$

where N_{ng} is the total nose load, which is usually taken as 10% of the total aircraft weight. Let Z_i and Z_k, respectively, represent amplitudes of the ith and kth random profiles at the same instant of time, and let S_y represent distance between contact points of two tires of NLG with the runway, then using the variation of Z in S_y units of the horizontal coordinate in space, the moment excitation $M_{\alpha\mathrm{ex}}$ generated about the x axis as a function of time at time t can be computed using the equation

$$M_{\alpha\mathrm{ex}} = K_\alpha \alpha_{\mathrm{ex}} \tag{5}$$

where

$$\alpha_{\mathrm{ex}} = \tan^{-1}\left(\frac{Z_i(t) - Z_k(t)}{S_y}\right) \tag{6}$$

The expression for $M_{\alpha\mathrm{ex}}$ given by Eq. (5), along with Eq. (6), provides the lateral excitation generated by the runway roughness on the NLG.

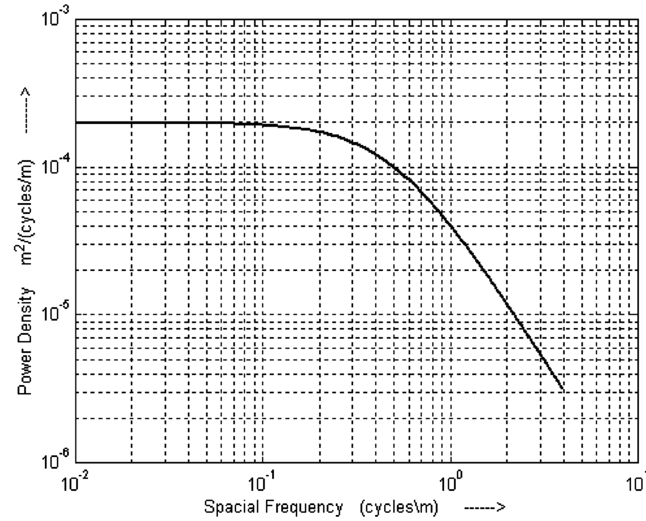

Fig. 2 PSD of rough-correlated profile ($\eta_{\mathrm{rc}} = 0.5 \times 10^{-4}$ and $\nu = 0.5$) at $V = 20$ m/s.

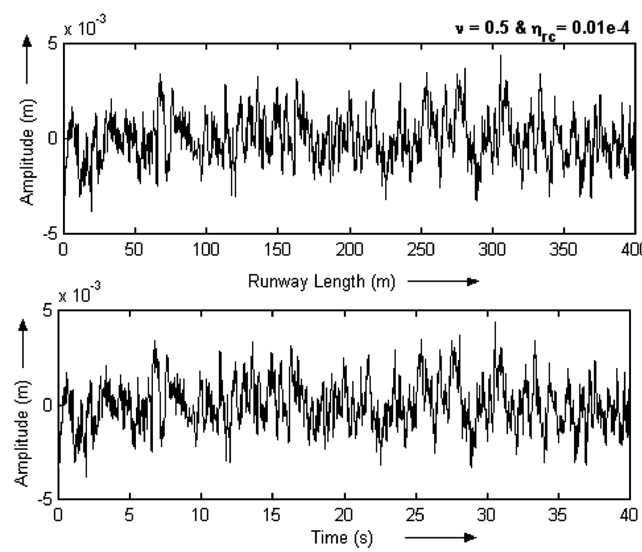

Fig. 3 Smooth-correlated runway profile.

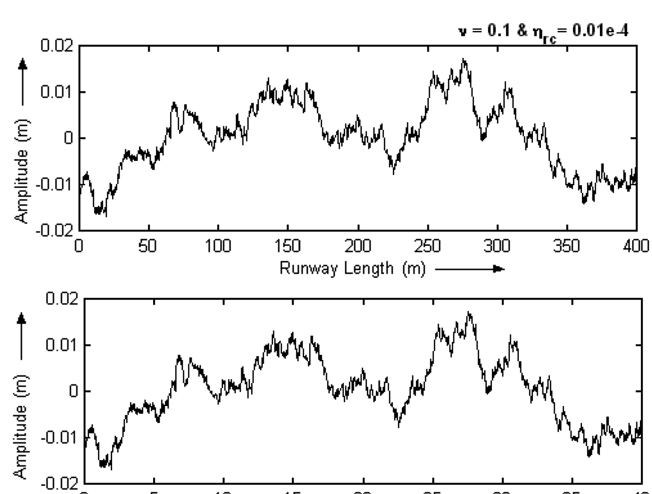

Fig. 4 Smooth-uncorrelated runway profile.

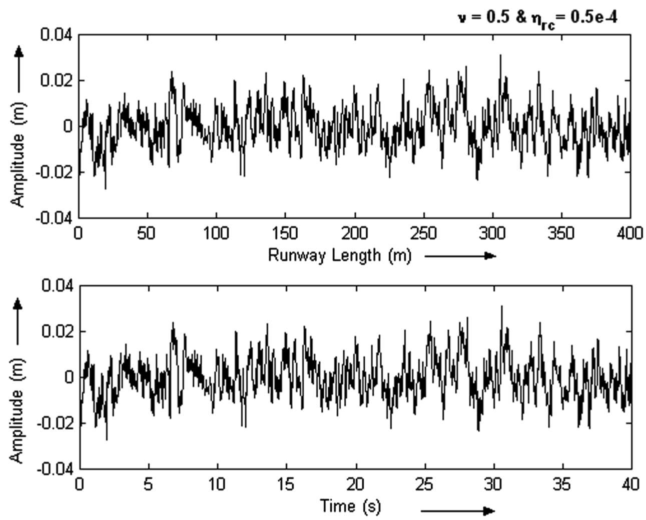

Fig. 5 Rough-correlated runway profile.

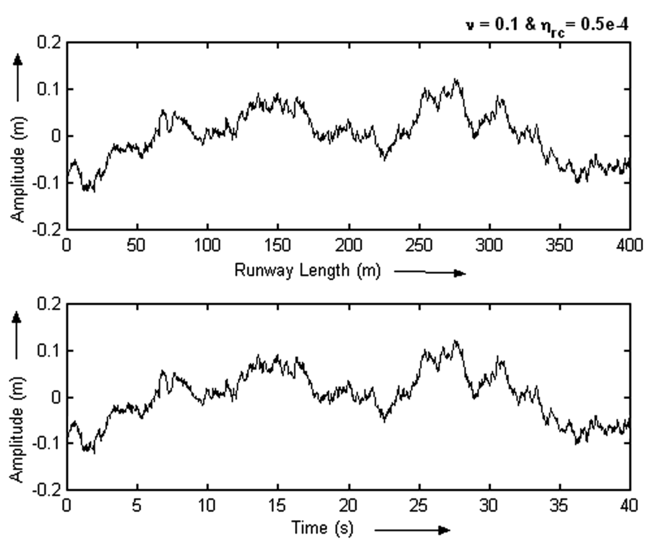

Fig. 6 Rough-uncorrelated runway profile.

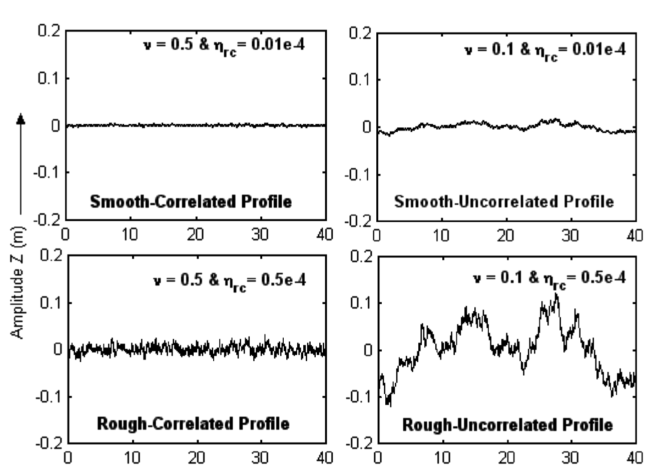

Fig. 7 Runway excitation amplitudes at $V = 10$ m/s for smooth-correlated to rough-uncorrelated profiles.

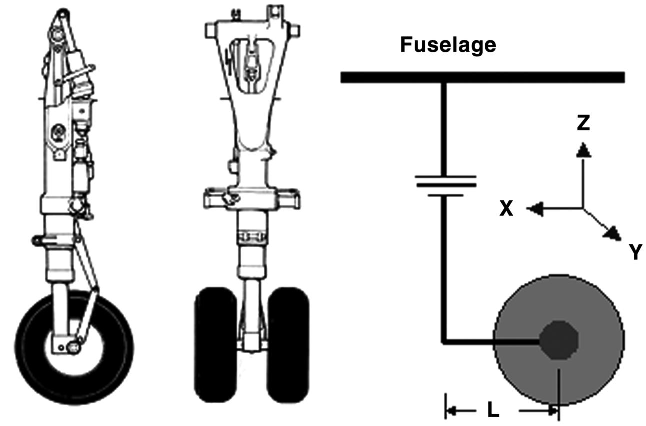

Fig. 8 Schematic of nose-wheel landing gear.

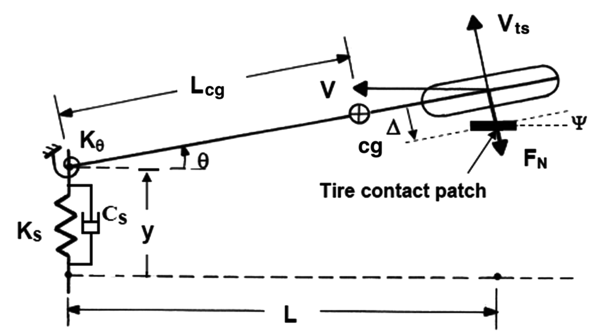

Fig. 9 Simplified nose-wheel landing gear model.

IV. Modeling NLG Lateral Dynamics with Runway Excitation

The mathematical model of the simplified NLG for linear analysis should account for the structural inertia, stiffness, and structural damping, along with proper mathematical relationships describing the force-deflection characteristics of the tire. Figure 8 shows a typical NLG configuration [21] and a schematic representation of the same as a cantilever support from the fuselage, with a rigid swiveling member of length L attached to a nonswiveling structure. Here, L is called the caster or trail of the NLG wheel, which is provided to have enough moment arm to drive the steering using hydraulic steering action. The landing gear flexibility may cause fore and aft motion, lateral motion in the y direction, and vertical motion absorbed by the oleopneumatic shock absorber. Landing gear may also rotate about the fore and aft axis (x axis) because of lateral bending. The wheel is free to swivel about the vertical axis when the steering is not engaged. This degree of freedom helps with steering the aircraft. The dynamics of symmetric NLG system consists of 1) uncoupled symmetric longitudinal dynamics involving fore and aft and up and down motions and rotation about the lateral axis (y axis) at the root and 2) uncoupled lateral dynamics, which involves lateral motion, rotation about the fore and aft axis (x axis), swiveling of the wheel assembly, and lateral and yaw deformations of the tire.

Consider a NLG model, as shown in Fig. 9, which has lateral displacement of the wheel y, angular wheel motion (yaw) about the vertical axis θ, lateral deflection of the tire contact patch with respect to wheel center plane Δ, roll of the wheel plane about the fore–aft axis α, and twist of the tire contact patch with respect to the wheel about the vertical axis ψ as DOF. The deformations of the tire are indicated by the deflection Δ and angle of twist ψ of the tire-contact-patch axis relative to the wheel plane. Several theoretical models for tire dynamics have been proposed and used in literature. The most realistic and useful of these are Moreland's point-contact model and von Schlippe's stretched-string model. In this study, mathematical relationships describing the force-deflection characteristics of the tire are based on the point-contact model. This model ignores tire inertias associated with tire deformations and uses a first-order model for side force F_N and the tire yawing (cornering) moment M_ψ. This theory accounts for the effect of side force on the yaw angle of the tire and a time delay between the application of the side force and the steady-state yaw. As the wheel rotates, when a side force is applied to the tire, it deflects laterally by Δ and changes its orientation with respect to the wheel plane by an angle ψ. This angle ψ is not developed instantaneously on the application of the lateral force F_N, but there is a time delay. Moreland [1] proposed a relationship between F_N and ψ to account for this delay in terms of a tire yaw coefficient C and a tire yaw time constant C_1, which is given by

$$CF_N = C_1\dot{\psi} + \psi \tag{7}$$

When there is a cornering moment M_ψ, tire twist ψ is produced about the vertical axis of the strut because of its torsional flexibility. Moreland [1] observed that the yaw angle ψ of the tire is also a function of the side force F_N produced by the deflection Δ. The side force F_N and the cornering moment M_ψ are given by

$$F_N = K_\Delta \Delta + C_\Delta \dot{\Delta} \tag{8}$$

$$M_\psi = K_\psi \psi + C_\psi \dot{\psi} \tag{9}$$

The total normal velocity of the wheel due to the combined effects of tire deformations is $V\psi + \dot{\Delta}$. The third source of normal velocity exists when the wheel is trailing the pivot with a lateral deformation y, an angle θ, with the direction of forward velocity of the airplane. When there is no tire slippage with respect to the ground (i.e., the total lateral velocity at the tire contact point due to the combined effects of tire deformations), wheel yaw and strut lateral deformations is zero and the total lateral deformation at the tire hub is absorbed by the tire deformation. Assuming θ to be small ($\sin\theta = \theta$), we have

$$\dot{y} + L\dot{\theta} - \dot{\Delta} + V(\theta - \psi) = 0 \tag{10}$$

This equation defines the kinematic condition when there is no lateral tire slip (i.e., $V_{ts} = 0$) and couples the tire dynamics with NLG strut dynamics. Let us consider a single-wheel NLG configuration as shown in Fig. 10. When the rolling of the wheel plane about the fore and aft axis is considered (Fig. 10a), because of ground reaction, the normal force will act at a point slightly off with respect to the vertical plane passing through the axle of the wheel. This produces a moment M_α in the roll direction about the fore and aft axis of the wheel and is given by

$$M_\alpha = -N(R\alpha - \Delta) \tag{11}$$

where N is the normal reaction of the ground and R is the rolling radius of the tire. Because of the rotation of the tire about its axle (caused by the forward motion of the wheel), the wheel will experience a tangential friction force that will produce a moment in the direction of wheel yaw equal to $\mu_r M_\alpha$, where μ_r is the rolling friction coefficient. When gear attitude angle γ (measured positive forward) is considered (see Fig. 10c) for the single-wheel configuration, the rolling moments about the fore and aft axis and yawing moment about the vertical axis are given by, respectively,

$$M_{sw_\alpha} = M_\alpha \cos\gamma - \mu_r M_\alpha \sin\gamma \tag{12}$$

$$M_{sw_\theta} = M_\alpha \sin\gamma + \mu_r M_\alpha \cos\gamma \tag{13}$$

Taking into account the forces due to wheel roll, tire twist, gear attitude angle, and wheel gyroscopic moments about the vertical and fore and aft axes and assuming θ to be small ($\cos\theta = 1$ and $\sin\theta = \theta$) and that there is no lateral tire slippage with respect to the ground, the equations of motion for the dynamics of the 5-DOF single-wheel NLG model can be written as

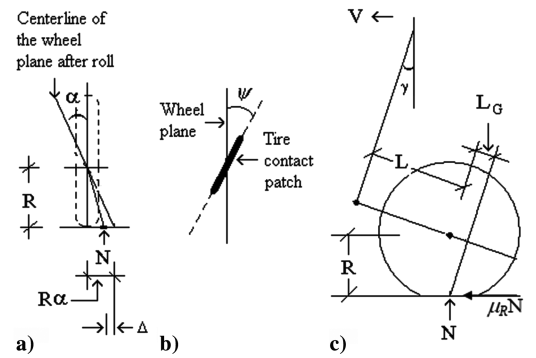

Fig. 10 Single-wheel nose landing gear model.

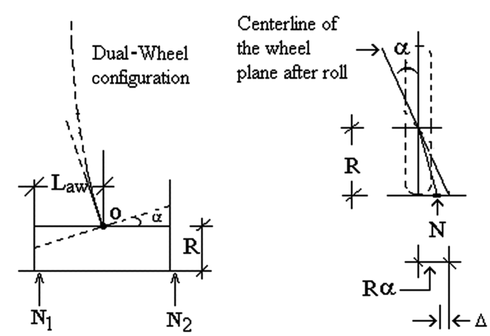

Fig. 11 Nose-wheel landing gear model with dual-wheel and gear attitude.

$$m\ddot{y} + mL_{cg}\ddot{\theta} + C_S\dot{y} + K_S y + F_N = 0 \tag{14}$$

$$I\ddot{\theta} + mL_{cg}\ddot{y} + (C_\theta + C_{Sh})\dot{\theta} + K_\theta\theta - (V/R)I_P\dot{\alpha} + M_{sw\theta} + M_\psi + F_N(L + R\sin\gamma) = 0 \tag{15}$$

$$I_\alpha\ddot{\alpha} + C_\alpha\dot{\alpha} + K_\alpha\alpha + M_{sw_\alpha} + (V/R)I_P\dot{\theta} + F_N R\cos\gamma = 0 \tag{16}$$

$$CF_N - (C_1\dot{\psi} + \psi) = 0 \tag{17}$$

$$\dot{y} + (L + R\sin\gamma)\dot{\theta} + R\dot{\alpha} - \dot{\Delta} + V(\theta - \psi) = 0 \tag{18}$$

In the preceding equations, $R\sin\gamma$ is called the geometric trail of the gear, and single and double dots over the quantities represent the first and second derivatives with respect to time t. Now consider a dual-wheel configuration, as shown in Fig. 11. In this case, it is necessary to account for the effect of the normal and tangential forces on the left and right wheels that act at a distance L_{aw} from the fore and aft axis. This results in additional moment components in the yaw and roll directions [22]. Assuming equal tire pressure in the tires (i.e., the value of vertical tire stiffness K_{Zt} of the tire is the same) and zero gear attitude angle γ, the moment about the fore and aft axis (opposing the direction of α) is given by

$$M_\alpha = N_1[L_{aw} - (R\alpha - \Delta)] - N_2[L_{aw} + (R\alpha - \Delta)] = M_{\alpha_1} + M_{\alpha_2} \tag{19}$$

where

$$N_1 = \frac{N}{2} + K_{Zt}L_{aw}\alpha, \qquad N_2 = \frac{N}{2} - K_{Zt}L_{aw}\alpha, \qquad M_{\alpha_1} = N(R\alpha - \Delta), \qquad M_{\alpha_2} = 2K_{Zt}L_{aw}^2\alpha \tag{20}$$

Considering the effect of gear attitude angle γ, the moment M_{dw_θ} about the axis of the strut and M_{dw_α} about the fore and aft axis for the dual-wheel configuration are given by

$$\begin{aligned} M_{\mathrm{dw}_\theta} &= (M_{\alpha_1} + M_{\alpha_2})\sin\gamma + \mu_r(M_{\alpha_1} + M_{\alpha_2})\cos\gamma \\ M_{\mathrm{dw}_\alpha} &= (M_{\alpha_1} + M_{\alpha_2})\cos\gamma - \mu_r(M_{\alpha_1} + M_{\alpha_2})\sin\gamma \end{aligned} \tag{21}$$

Accounting for the preceding dual-wheel model, Eqs. (15) and (16) can be modified as

$$\begin{aligned} & I\ddot{\theta} + mL_{\mathrm{cg}}\ddot{y} + (C_\theta + C_{\mathrm{Sh}})\dot{\theta} + K_\theta\theta - (V/R)I_P\dot{\alpha} + M_{\mathrm{dw}\theta} \\ & \quad + M_\psi + F_N(L + R\sin\gamma) = 0 \end{aligned} \tag{22}$$

$$I_\alpha\ddot{\alpha} + C_\alpha\dot{\alpha} + K_\alpha\alpha + M_{\mathrm{dw}_\alpha} + (V/R)I_P\dot{\theta} + F_N R\cos\gamma = 0 \tag{23}$$

It is assumed that free play in torsion is the only source of nonlinearity in the NLG; the free play is modeled as a nonlinear relationship between the torsional moment M_θ and wheel rotation θ (expressed in terms of torsional stiffness K_θ) and free play in wheel rotation θ_{fp}. This is given by

$$\begin{aligned} M_\theta &= 0 && -\theta_{\mathrm{fp}} < \theta < \theta_{\mathrm{fp}} \\ M_\theta &= K_\theta(\theta - \theta_{\mathrm{fp}}) && \theta > \theta_{\mathrm{fp}} \\ M_\theta &= K_\theta(\theta + \theta_{\mathrm{fp}}) && \theta < -\theta_{\mathrm{fp}} \end{aligned} \tag{24}$$

Then the dynamic equations of motion for the 5-DOF nonlinear dual-wheel nose gear model with gear attitude and wheel gyroscopic forces accounting for runway excitation and torsional free play can be written in matrix form as

$$\begin{aligned} & \begin{bmatrix} K_S & 0 & 0 & K_\Delta & 0 \\ 0 & 0 & (2K_{Zt}L_{aw}^2 - N'R)(\sin\gamma + \mu_r\cos\gamma) & N'(\sin\gamma + \mu_r\cos\gamma) + K_\Delta(L + R\sin\gamma) & K_\psi \\ 0 & 0 & (2K_{Zt}L_{aw}^2 - N'R)(\cos\gamma - \mu_r\sin\gamma) + K_\alpha & N'(\cos\gamma - \mu_r\sin\gamma) + K_\Delta R\cos\gamma & 0 \\ 0 & 0 & 0 & -CK_\Delta & 1 \\ 0 & V & 0 & 0 & -V \end{bmatrix} \begin{Bmatrix} y \\ \theta \\ \alpha \\ \Delta \\ \Psi \end{Bmatrix} \\ & + \begin{bmatrix} C_S & 0 & 0 & C_\Delta & 0 \\ 0 & C_\theta + C_{\mathrm{Sh}} & -(V/R)I_P & C_\Delta(L + R\sin\gamma) & C_\psi \\ 0 & (V/R)I_P & C_\alpha & C_\Delta R\cos\gamma & 0 \\ 0 & 0 & R & -CC_\Delta & C_1 \\ 1 & L + R\sin\gamma & R & -1 & 0 \end{bmatrix} \begin{Bmatrix} \dot{y} \\ \dot{\theta} \\ \dot{\alpha} \\ \dot{\Delta} \\ \dot{\Psi} \end{Bmatrix} + \begin{bmatrix} m & mL_{\mathrm{CG}} & 0 & 0 & 0 \\ mL_{\mathrm{CG}} & I & 0 & 0 & 0 \\ 0 & 0 & I_\alpha & 0 & 0 \\ 0 & 0 & 0 & 0 & 0 \\ 0 & 0 & 0 & 0 & 0 \end{bmatrix} \begin{Bmatrix} \ddot{y} \\ \ddot{\theta} \\ \ddot{\alpha} \\ \ddot{\Delta} \\ \ddot{\Psi} \end{Bmatrix} = -\begin{Bmatrix} 0 \\ M_\theta \\ M_{\alpha_{\mathrm{ex}}} \\ 0 \\ 0 \end{Bmatrix} \end{aligned} \tag{25}$$

where $N' = N - F_{\mathrm{zex}}$, and F_{zex} and $M_{\alpha\mathrm{ex}}$ are given by Eqs. (4) and (5), respectively. In the preceding equation, the nonhomogeneous term $M_{\alpha\mathrm{ex}}$ represents the moment excitation produced in the direction of α by the runway roughness, coupled with the nonlinear lateral dynamics of NLG.

V. Results and Discussion

It can be seen from the literature [23–25] that for the dynamics of nonlinear structural systems, the Newmark-β and the Runge–Kutta methods are the most widely used. The response of the NLG models to ground-induced excitation is obtained by integrating the equations of system dynamics using the Newmark-β scheme. Responses are obtained for linear and nonlinear systems in terms of the variation of y, θ, and Δ with time. Results are obtained for runway profiles of different roughness and correlation coefficients. Forced-response studies are carried out for the nonlinear NLG system with free play. The results presented here correspond to the NLG parameters shown in Table 1. The values of the roughness coefficient considered in the present study cover a wide range from smooth to rough and cover runway classes from poor to good.

A. Response Studies on Linear Systems

Fig. 12 shows time responses in terms of y, θ, and Δ for typical subcritical and postcritical velocities for the linear five DOF dual-wheel NLG model for the case of a smooth-correlated surface ($\eta_{\mathrm{rc}} = 10^{-6}$ and $\nu = 0.5$). For this system, it can be seen from Fig. 13 that $V = V_{\mathrm{Cr}} = 280$ kmph. Figure 13 also shows peak lateral accelerations at various velocities for the linear system, with runway excitation due to various runway conditions ranging from smooth-correlated to rough-uncorrelated profiles. It is observed that unacceptable levels of lateral accelerations may be caused by roughness, even at subcritical velocities. Increased runway roughness can thus effectively bring down the margin available between the maximum taxi velocities and their limiting values.

B. Response Studies on Nonlinear Systems

Figure 14 shows forced responses in terms of y, θ, and Δ for two typical velocities for the nonlinear NLG model with free play for the case in which $\theta_{\mathrm{fp}} = 5 \times 10^{-4}$ rad, $\eta_{\mathrm{rc}} = 0.01 \times 10^{-4}$, and $\nu = 0.5$. Figure 15 shows the corresponding phase–plane plots in terms of y and $\dot{y}$. Figure 16 shows a comparison of peak lateral accelerations at various velocities for the linear model without free play and nonlinear model with free play ($\theta_{\mathrm{fp}} = 5 \times 10^{-4}$ rad) for the cases in which $\nu = 0.5$ and $\eta_{\mathrm{rc}} = 0.01 \times 10^{-4}$ (smooth) and 0.1×10^{-4} (moderately rough) and 0.5×10^{-4} (rough). Figure 17 shows steady-state free-vibration responses in the absence of runway excitation ($\eta_{\mathrm{rc}} = \nu = 0$), giving values of lateral acceleration at various velocities for the NLG system with free play for the case in which $\theta_{\mathrm{fp}} = 5 \times 10^{-4}$ rad. It can be seen from Fig. 17 that the NLG system is dynamically stable up to a value of velocity (60 kmph), beyond which limit-cycle oscillations are observed as significant lateral accelerations. This response becomes unstable as the critical divergence velocity (183 kmph) is approached. In the presence of runway excitation, as shown by Fig. 16, the NLG system with free play shows 1) small self-limiting oscillations in the dynamically stable region, 2) large self-sustaining oscillations in the velocity range between the onset of limit cycle and divergence, and 3) divergent response as the critical velocity is reached. It is seen from the preceding results that free play by itself causes a very significant reduction in the critical divergence velocity and that free play and runway excitation in combination have a more adverse effect.

Table 1 Values of NLG and runway parameters for baseline problem and their ranges

	Baseline values of parameters
Strut inertia parameters	$m = 22$ kg, $N = 10$ kN, and $I_{cg} = 0.198$ kgm^2
Strut geometric parameters	$L = 0.075$ m, $L_{cg} = 0.0675$ m, $R = 0.175$ m, $\theta_{fp} = 0.0005$ rad, and $\gamma = 0$ deg
Strut stiffness parameters	$K_S = 542.83$ kN/m, $\Omega = 3$, and $K_\alpha = 400$ kN/m
Strut damping parameters	$C_S = 1\%$, $C_\theta = 2\%$, and $C_{Sh} = 0$
Tire parameters	$K_\Delta = 238.75$ kN/m, $C_\Delta = 205$ Ns/m, $K_\psi = 665$ Nm/rad, $C_\psi = 0.7$ Nms/rad, $C_1 = 0.0010886$ s, $C = 2.356 \times 10^{-5}$ rad/N, and $K_{Zt} = 250$ kN/m
Runway parameters	$\mu_r = 0.02$, $\eta_{rc} = 0.01 \times 10^{-4}$ and $\nu = 0.5$
	Range of values of parameters
Forward velocity	$V = 0$–300 kmph
Runway parameters	$\eta_{rc} = 0.01 \times 10$–$4 \times 0.5 \times 10^{-4}$ and $\nu = 0.1$–0.5

VI. Conclusions

Analytical formulation for the lateral dynamics of linear and nonlinear NLG models and simulation of their time-domain response to runway-induced excitation was presented. Using simulated runway profiles obtained as a combination of randomly phased sinusoids with specified spectral characteristics and considering a dual-wheel configuration for the NLG, lateral excitation was obtained as a rolling moment varying with time. Numerical studies were carried out to bring out the effect of runway roughness and its interaction with torsional free play. These results show that the critical velocity for divergent response is lowered by runway excitation and is dependent on the runway roughness. The results also show that free play by itself causes a very significant reduction in the critical divergence velocity and that free play and runway

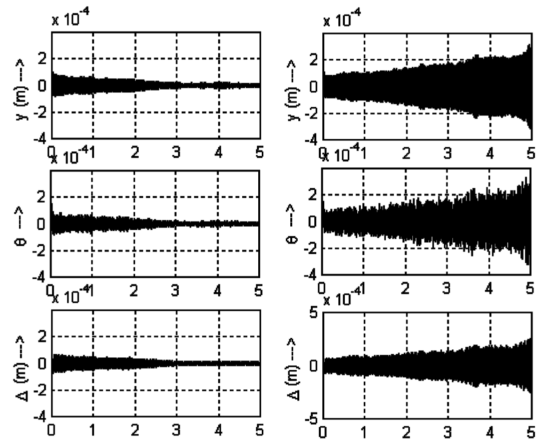

Fig. 12 Time responses in terms of y, θ, and Δ before and after the onset of shimmy for the linear 5-DOF dual-wheel NLG model with runway excitation for the case $\eta_{rc} = 0.01 \times 10^{-4}$ and $\nu = 0.5$ at a) $V = 270$ kmph and b) $V = 288$ kmph.

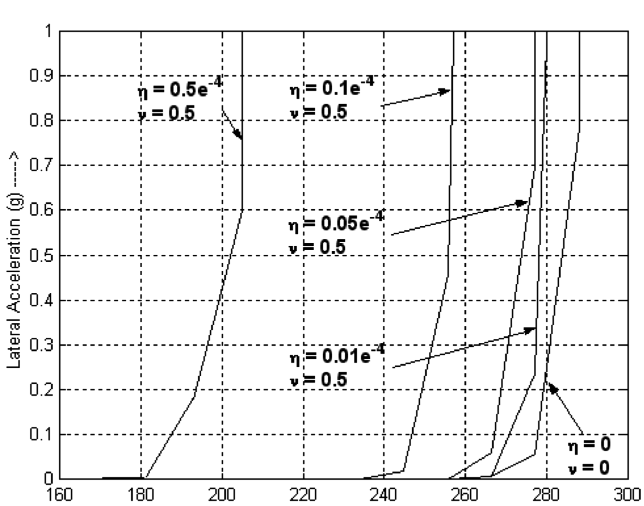

Fig. 13 Peak lateral accelerations at various velocities for the linear 5-DOF dual-wheel NLG model with runway excitation for the case $\nu = 0.5$ and $\eta_{rc} = 0.01 \times 10^{-4}$–$0.5 \times 10^{-4}$.

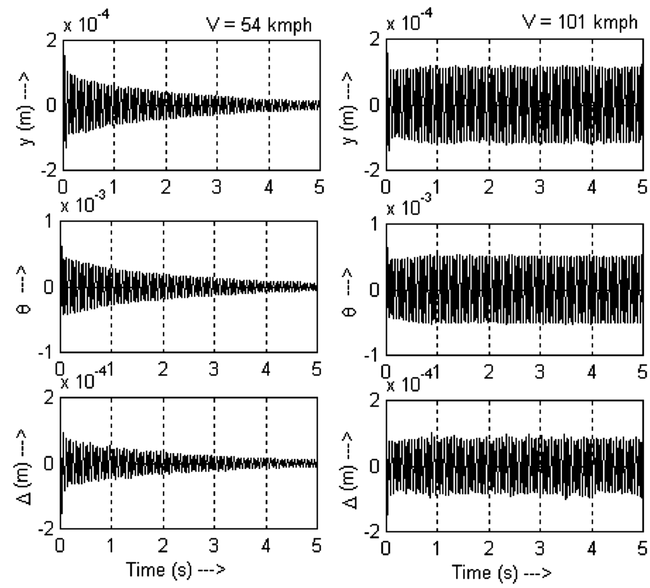

Fig. 14 Time responses in terms of y, θ, and Δ for the nonlinear 5-DOF dual-wheel NLG model with runway excitation and free play at $V = 54$ and 101 kmph for the case $\theta_{fp} = 5 \times 10^{-4}$ rad, $\eta_{rc} = 0.01 \times 10^{-4}$, and $\nu = 0.5$.

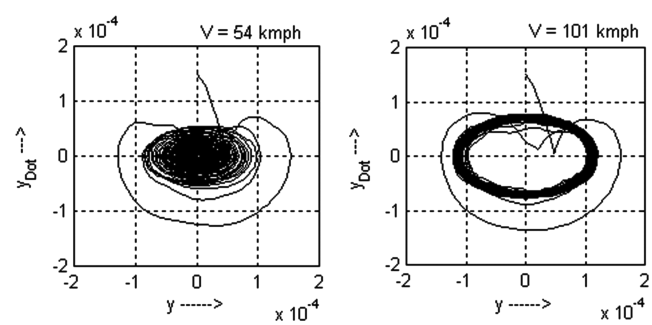

Fig. 15 Phase–plane plots of y for the nonlinear NLG model with runway excitation at $V = 54$ and 101 kmph for the case $\theta_{fp} = 5 \times 10^{-4}$ rad, $\eta_{rc} = 0.01 \times 10^{-4}$, and $\nu = 0.5$.

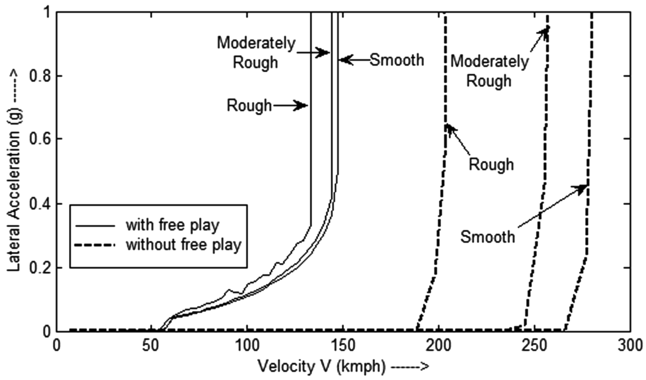

Fig. 16 Comparison of peak lateral accelerations at various velocities for the linear model without free play and nonlinear model with a free play ($\theta_{fp} = 5 \times 10^{-4}$ rad) for the case $\nu = 0.5$ and $\eta_{rc} = 0.01 \times 10^{-4}$ (smooth), 0.1×10^{-4} (moderately rough) and 0.5×10^{-4} (rough).

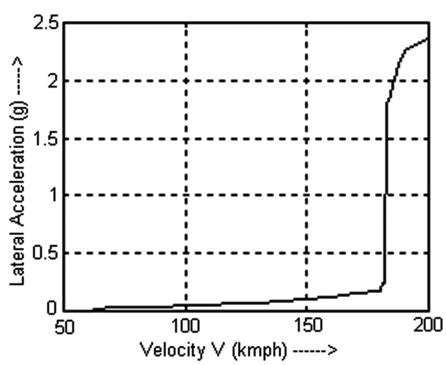

Fig. 17 Steady-state amplitude values of lateral acceleration at various velocities for the NLG system without runway excitation for the case $\theta_{fp} = 5 \times 10^{-4}$ rad ($V_{Cr} = 183$ kmph).

excitation in combination have a more adverse effect. The preceding studies bring out the need for such simulations in estimating the operational ranges of aircraft velocities during ground roll.

Acknowledgments

The work presented here is included in the Ph.D. thesis [26] of the first author and was carried out as a sponsored research project funded by the Aeronautical Development Agency, Bangalore, India. Valuable discussions with the Structures Group of the Aeronautical Development Agency and the Landing Gear Group of Hindustan Aeronautics Limited, Bangalore are gratefully acknowledged.

References

[1] Moreland, W. J., "The Story of Shimmy," *Journal of the Aeronautical Sciences*, Vol. 21, No. 12, Dec. 1954, pp. 793–808.

[2] Walter, B., and Howard, Jr., "A Full-Scale Investigation of the Effect of Several Factors on the Shimmy of Castering Wheels," NACA TN-760, Apr. 1940.

[3] Krabacher, W. E., "A Review of Aircraft Landing Gear Dynamics," AGARD Rept. R-800, Mar. 1996.

[4] Krabacher, W. E., "Comparison of the Moreland and Von Schlippe-Dietrich Landing Gear Tire Shimmy Models," *Vehicle System Dynamics*, Vol. 27, Sept. 1997, pp. 335–338. doi:10.1080/00423119708969667

[5] Baumann, J., "A Non-Linear Model for Landing Gear Shimmy with Applications to the McDonnell Douglas F/A-18A," AGARD Rept. R-800, Mar. 1996.

[6] Li, G. X., "Modelling and Analysis of a Dual-Wheel Nose Gear: Shimmy Instability and Impact Motions," *Proceedings of the SAE Aerospace Atlantic Conference and Exposition*, Society of Automotive Engineers, Warrendale, PA, 20–23 Apr. 1993, pp. 129–143.

[7] Gordon, J. T., Jr., and Merchant, H. C., "An Asymptotic Method for Predicting Amplitudes of Non-Linear Wheel Shimmy," *Journal of Aircraft*, Vol. 55, No. 3, Mar. 1978, pp. 155–159.

[8] Koenig, K., "Unsteady Tire-Dynamics and the Application Thereof to Shimmy and Landing Load Computations," AGARD Rept. R-800, Mar. 1996.

[9] Sura, N. K., and Suryanarayan, S., "Stability and Response Studies on Simplified Linear Models of Nose-Wheel Landing Gears," *Journal of Aerospace Sciences and Technologies*, Vol. 56, No. 1, Feb. 2004, pp. 49–54.

[10] Sura, N. K., and Suryanarayan, S., "Closed Form Analytical Expressions for Shimmy Velocity and Frequency of Nose Wheel Landing Gear," *Proceedings of the International Conference on Theoretical, Applied, Computational and Experimental Mechanics* [CD-ROM], Indian Inst. of Technology, Kharagpur, India, 28–30 Dec. 2004, Paper 721302.

[11] Sura, N. K., and Suryanarayan, S., "Dynamic Response and Stability Studies on Simplified Models of Aircraft Landing Gears," *Proceedings of the India-USA Symposium on Emerging Trends in Vibration and Noise Engineering* [CD-ROM], The Ohio State Univ., Columbus, OH, 10–12 Dec. 2001, Paper U048.

[12] Sura, N. K., Suryanarayan, S., Dipak K. M., and Upadhya, A. R., "Stability and Response Studies on Non-Linear Models of Nose-Wheel Landing Gears," *Proceedings of Aerospace and Related Mechanisms 2002*, Vikram Sarabhai Space Center, Trivendrum, Kerala, India, 8–9 Nov. 2002, pp. 238–242.

[13] Sura, N. K., and Suryanarayan, S., "Stability and Response Studies on Simplified Models of Nose-Wheel Landing Gear with Hard Tires," *Journal of the Institution of Engineers (India)*, Vol. 85, May 2004, pp. 29–36; also available online at http://www.ieindia.org/publish/as/0504/may04as5.pdf.

[14] Yadav, D., and Kapadia, K. E., "Non-Homogeneous Track-Induced Response of Vehicles with Non-Linear Suspension During Variable Velocity Runs," *Journal of Sound and Vibration*, Vol. 143, No. 1, 1990, pp. 51–64. doi:10.1016/0022-460X(90)90567-J

[15] Yadav, D., and Nigam, N. C., "Ground Induced Non-Stationary Response of Vehicles," *Journal of Sound and Vibration*, Vol. 61, No. 1, 1978, pp. 117–126. doi:10.1016/0022-460X(78)90046-9

[16] Rassaian, M., "Power Spectral Density Conversions and Nonlinear Dynamics," *Shock and Vibration*, Vol. 1, No. 4, 1994, pp. 349–356.

[17] Harrison, R. F., and Hammond, J. K., "A Systems Approach to the Characterization of Rough Ground," *Journal of Sound and Vibration*, Vol. 99, No. 3, 1985, pp. 437–447. doi:10.1016/0022-460X(85)90380-3

[18] Harrison, R. F., and Hammond, J. K., "Evolutionary (Frequency/Time) Spectral Analysis of the Response of Vehicles Moving on Rough Ground by Using Covariance Equivalent Modelling," *Journal of Sound and Vibration*, Vol. 107, No. 1, 1986, pp. 29–38. doi:10.1016/0022-460X(86)90280-4

[19] Harrison, R. F., and Hammond, J. K., "Approximate Time Domain, Non-Stationary Analysis of Stochastically Excited, Non-Linear Systems with Particular Reference to the Motion of Vehicles on Rough Ground," *Journal of Sound and Vibration*, Vol. 105, No. 3, 1986, pp. 361–371. doi:10.1016/0022-460X(86)90165-3

[20] Rajesh, M., "Time Domain Simulation Studies on Response of Flexible Aircraft to Gust Spectra," M.Tech. Dissertation, Aerospace Engineering Dept., Indian Inst. of Technology Bombay, Mumbai, Jan. 2003.

[21] Young, D. W., "Aircraft Landing Gears—The Past Present and Future," Society of Automotive Engineers, Paper 864752, July 1985.

[22] Glaser, J., and Hrycko, J., "Landing Gear Shimmy—De Havilland's Experience," AGARD Rept. R-800, Mar. 1996.

[23] Bathe, K. J., *Finite Element Procedures in Engineering Analysis*, Prentice–Hall, Englewood Cliffs, NJ, 1982.

[24] Berg Glen, V., *Elements of Structural Dynamics*, Prentice–Hall, Englewood Cliffs, NJ, 1989.

[25] Xie, Y. M., "An Assessment of Time Integration Schemes for Non-Linear Dynamic Equations," *Journal of Sound and Vibration*, Vol. 192, No. 1, 1996, pp. 321–331. doi:10.1006/jsvi.1996.0190

[26] Sura, N. K., "Lateral Stability and Response of Nose Wheel Landing Gears," Ph.D. Dissertation, Aerospace Engineering Dept., Indian Inst. of Technology, Bombay, Mumbai, India, Sept. 2004.

T. Augustine
Associate Editor